Characterization of Trailing Vortices Generated by a Rushton Turbine

Renaud Escudié, Denis Bouyer, and Alain Liné
Laboratoire d'Ingénierie des Procédés de l'Environnement, Institut National des Sciences Appliquées de Toulouse, 31077 Toulouse Cedex, France

The discharge flow of a Rushton turbine is characterized by a counter-rotating vortex pair generated behind the impeller blade. The objective here is to characterize these trailing vortices. To this end, PIV measurements were synchronized with blade position. These measurements were performed to identify and locate the trailing vortices, according to an identification technique proposed to detect a vortical region. The advantage of this method for determining the trailing vortex is highlighted after comparison to previous techniques. The trajectory of the vortices is deduced and it is shown to follow the phase-averaged velocity field induced by the impeller. The trailing vortices were characterized in terms of size and velocity circulation within the vortex. The interactions between these organized structures and turbulence were also illustrated. © 2004 American Institute of Chemical Engineers *AIChE J,* 50: 75–86, 2004
Keywords: mixing, agitated tank, trailing vortex, Rushton turbine

Introduction

In a stirred vessel, the flow field generated by a Rushton turbine is complex. The discharge flow of the impeller is characterized both by a high level of turbulence and by coherent vortical structures induced by the blade motion.

These trailing vortices were identified by the pioneering works of Van't Riet and Smith (1973, 1975) and Van't Riet et al. (1976) who described a counter-rotating vortex pair generated behind the lower and upper sides of the impeller blades. Yianneskis (2000) gave a clear explanation of tip vortices generation: *the pressure gradient in the region near the tip of a finite span wing produces a transverse flow which winds around the tip to form a tip vortex. The vortex is continuously fed by the roll-up of the vortex sheet issuing from the trailing edge of the wing.*

Indeed, trailing vortices have significant impact on mixing tanks:

- Vortices can affect impeller efficiency: minimizing vortex size improves the blending performance of an impeller;
- Vortices provide a source of turbulence (Escudié, 2001; Bouyer, 2002); and
- In an aerated tank, different kinds of gas cavities are generated in the trailing vortex region.

In the past, the analysis of trailing vortices has been mainly descriptive. The localization of a vortex core is actually difficult, in particular in turbulent flow. In order to define and identify the vortical structures, the techniques of Jeong and Hussain (1995) will be followed. These authors reviewed the question of definition and identification of the vortical region. They pointed out that two requirements must be satisfied to identify a vortex:

- Requirement No. 1: a vortex must have a net vorticity,
- Requirement No. 2: the identification scheme must be a Galilean invariant.

Thus, Jeong and Hussain (1995) proposed a new definition of a vortex. It is based on the eigenvalues of the tensor $S^2 + \Omega^2$, where S and Ω are, respectively, the symmetric and the antisymmetric parts of the velocity gradient tensor $\nabla \otimes u$. They compared their identification technique with prior ones for a variety of laminar and turbulent flow: only their definition was found to represent correctly the geometry of the vortex core. This approach will be applied in the present study.

The analysis of the bibliography will focus on three points: a

Correspondence concerning this article should be addressed to A. Liné at line@insa-tlse.fr.

decomposition technique developed to extract organized motions from fluctuations; identification of trailing vortices in the mixing tank; and trajectory of trailing vortices in the mixing tank.

Decomposition technique

Near the impeller, the instantaneous velocities show different kinds of fluctuations: some fluctuations are purely turbulent, and others are due to the organized motion induced by the periodic motion of the blades of the impellers (related to trailing vortices). Different techniques have been used to separate coherent structures from random turbulence:

- Temporal or spectral analysis of velocity data in terms of velocity correlation functions (Mujumbar et al., 1970; Wu and Patterson, 1989) or energy spectra. In this technique, large amplitude peaks can be detected at the impeller frequency (Cutter, 1966; Van der Molen and Van Maanen, 1978; Costes and Couderc, 1988; Mahouast et al., 1989).
- Another way is to synchronize the acquisitions of velocity data with the blade position, in order to estimate phase averaged velocity components (Van der Molen and Van Maanen, 1978; Yianneskis et al., 1987, 1993; Stoots and Calabrese, 1995; Lee and Yianneskis, 1998; Schaffer et al., 2000; Sharp and Adrian, 2001; Escudié, 2001; Bouyer, 2002; Escudié and Liné, 2003).

The turbulent kinetic energy and the organized motion kinetic energy can thus be obtained (Cutter, 1966; Wu and Patterson, 1989; Mahouast et al., 1989; Escudié and Liné, 2003). In the impeller tip region, the kinetic energy of the organized motion is significant. In the region of the jet induced by the impeller, the following characteristics can be pointed out: the kinetic energy of the organized motion decreases whereas the turbulent kinetic energy increases. At a certain radial position, the kinetic energy of the organized motion vanished and, thereafter, the turbulence decreases. Van der Molen and Van Maanen (1978) suggested that a link seems to exist between turbulence and trailing vortices, because phase-averaged measurements have shown that the turbulent kinetic energy is higher in the trailing vortex region than elsewhere in the jet (Lee et Yianneskis, 1998; Schaffer et al., 1997; Ranade et al., 2001; Sharp et Adrian, 2001). Escudié and Liné (2003) have shown that kinetic energy is transferred from the organized motion to the turbulent one. This result will be illustrated in the last section of this article.

Identification of trailing vortices

A lot of research work has been devoted to identifying and characterizing the three-dimensional (3-D) structure of the vortices in the stream of the turbine.

A rotating frame of reference can be used to visualize the organized structures. Van't Riet and Smith (1973, 1975) mounted a camera on a turntable that rotated at the impeller rate. They identified the vortex zone and the circumferential velocity thanks to the trajectory of tracer particles. They studied the influence of Reynolds number Re defined as follows

$$Re = \frac{ND^2}{\nu} \tag{1}$$

They concluded that organized structures are only generated in the range $150 < Re < 250$.

A first method used to visualize the trailing vortex is based on phase-averaged velocity fields. This method is visual and qualitative. The second method used to identify the trailing vortex core is based on the resulting net vorticity (requirement 1). Using a large number of LDV measurements, Derksen et al. (1999) and Schaffer et al. (2000) characterized the vortex size in a vertical plane of measurement relative to the blade position, considering a dimensionless vorticity defined as follows

$$\xi = \omega \frac{T}{U_{tip}} \tag{2}$$

In this relationship, T refers to the tank diameter and U_{tip} to the velocity of the impeller tip. ω represents the dimensional vorticity in the vertical plane derived from experiments. In fact, a threshold ξ_c must be fixed arbitrarily to identify the contour of the trailing vortices. Schaffer et al. (2000) proposed different magnitudes of the identifier's threshold: $\xi_c = 13$ for a Rushton turbine, $\xi_c = 7$ for a pitch blade turbine, and $\xi_c = 10$ for an hydrofoil impeller. This criterion, thus, introduces some subjectivity. The limits of this method will be shown in this article. The effectiveness of the technique proposed by Jeong and Hussain (1995) in determining the region of trailing vortices will be established. The results will be exploited in terms of vortex size and velocity circulation.

Trajectory of trailing vortices

The trajectory of the trailing vortices has been investigated in the tanks. Van't Riet and Smith (1975) showed that the position of the vortex axis is independent of Re in turbulent regime $Re > 5\ 10^3$. Lee and Yianneskis (1998) compared the location of the vortex axis in the impeller stream jet deduced from several investigations reported in the literature and found some inconsistencies. The inconsistencies of the results may be caused by small differences in the stirred vessel configuration: clearance C between the impeller and the bottom of the tank, shaft diameter, blade and disc thickness (t_b and t_d) (Rutherford et al., 1996). However, the origin of the discrepancies may also be related to the identification method (requirement 2).

In more recent works, two methods were commonly used to localize vortex trajectory. The two methods are based on phase averaged velocity data (Yianneskis et al., 1987; Stoots and Calabrese, 1995; Lee and Yianneskis, 1998). In the first method, as the vertical displacement of the trailing vortices is small, the vortex axis is defined by the location where the vertical velocity is null. The second method is based on the location of the maximum vorticity magnitude.

The effectiveness of both the second method and the technique proposed by Jeong and Hussain (1995) in determining the trajectory of trailing vortices will be demonstrated in this article. In addition, the trajectory of the vortices will be shown to follow the phase-averaged velocity field induced by the impeller. It confirms that inconsistencies in the results observed by Lee and Yianneskis (1998) may have been caused by small differences in the stirred vessel geometry.

The objective of this article is to identify trailing vortices generated by a Rushton turbine, according to the method proposed by Jeong and Hussain (1995). To this end, PIV acquisitions were synchronized with the blade position. As it is

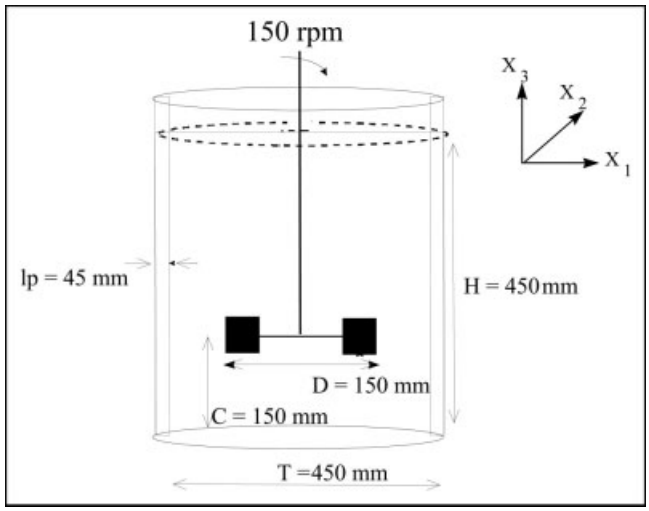

Figure 1. Tank geometry.

necessary to evaluate the gradient velocity tensor $\nabla \otimes u$, PIV measurements were performed in three planes: vertical, transversal, and horizontal. Once trailing vortices have been identified, the second objective of this study is to characterize the trailing vortices: trajectories, sizes, and velocity circulation within the vortex. These results will enable to illustrate the interaction between trailing vortices and turbulence to be illustrated.

The results will be presented in three parts: velocity database and vortex identification technique; identification of trailing vortices in mixing tanks; and characteristics of trailing vortices in mixing tanks: trajectory, velocity circulation.

Velocity Database and Vortex Identification Technique

Experimental apparatus

Measurements were taken in a standard cylindrical tank with an inside diameter $T = 450$ mm (Figure 1). The flat-bottom tank, filled with tap water up to a level $H = T = 450$ mm, was open at the top. The four equally spaced baffles were each one-tenth of the tank diameter in width ($B = T/10 = 45$ mm). The Rushton turbine (diameter $D = T/3 = 150$ mm) was mounted with a bottom clearance of $C = D = 150$ mm. The blade height w is $0.2D$; both the blade thickness t_b and the disk thickness t_d are equal to 2 mm. The impeller speed was 150 rpm in a clockwise direction as viewed from above. To minimize optical refraction, the vessel is placed in a cubic tank filled with tap water. An encoder is mounted on the shaft of the Rushton turbine in order to synchronize the acquisition of velocity data with the blade position.

PIV technique

The PIV system used in this study is the commercial system acquired from Dantec Measurement Technology. This technique enables an instantaneous 2-D velocity field in a plane to be acquired. The basic idea is that the fluid particle velocity can be calculated as long as it is possible to measure the displacement of fluid particles in a given time interval. The PIV technique is thus based on the following steps: seeding the fluid flow volume under investigation with a few micron-sized particles, which are assumed to closely follow the fluid flow, illuminating a slice of the flow field with a pulsing light sheet; recording two images of the fluid flow with a short time interval between them, using a digital CCD camera; processing these two successive images to get the instantaneous velocity field. The whole image is divided into interrogation areas. An intercorrelation technique is used to evaluate the most probable displacement of the seeding particles within each interrogation area.

The system includes a laser (Mini Yag, 15 Hz, 30 mJ), a double image recorder camera (Kodak Megaplus ES 1.0, 1024×1024 pixels), a dedicated processor (PIV 2000), and Flowmanager 3.40 software. The processor makes all the calculations in real time. As the processor produces vector maps, these are displayed and optionally stored by the software. The seeding material is made of spherical glass hollow silvered particles from Dantec (density = 1.4, $10\ \mu m < d_p < 30\ \mu m$). Interrogation areas are squares of 32×32 pixels.

Accuracy of data acquisition

The accuracy of velocity measurements depends on different parameters, such as the seeding concentration, the size of PIV measurement area, the time interval between two laser sheets, and the spatial resolution. For the same data bank, Escudié and Liné (2003) explained the choice of the PIV experimental conditions. The size of the measurement area (60×60 mm^2) is shown to not filter energetic scales. The size of the 32-pixels-by-32-pixels interrogation area is 2.2×2.2 mm^2. As the interrogation areas overlap by 50%, a vector is measured each 1.1 mm. Indeed, the Taylor microscale λ_T ranges between 0.5 and 1 mm and corresponds to the order of magnitude of the spatial resolution in the current experiment. The seeding concentration is adjusted to have between 5 and 10 particles in the interrogation region. The statistical averaging of the data was performed on a series of 1,000 instantaneous velocity fields and the statistical convergence was checked on mean velocity, Reynolds stress components and third-order moments of fluctuating velocity.

Measurement planes

The measurement area is limited to the region close to the Rushton turbine tip (Figure 2). The measurement plane is a bisector plane between two baffles. In order to calculate all the components of the velocity gradient tensor $\nabla \otimes u$, it is necessary to have values of the three velocity components in the three directions of the frame of reference. As a consequence, measurement in three different planes were performed: a vertical-radial plane (X_1-X_3 plane), nine vertical-tangential planes (X_1-X_2 plane) 5 mm spaced, nine horizontal planes (X_2-X_3 plane) 5 mm spaced also. In each plane, a vector is measured each 1.1 mm. As a consequence, the experimental data are localized in a geometrical domain, for a normalized radial position r/R ranging between 1.06 and 1.6, and for an normalized vertical position $2z/w$ ranging between -1.3 and 1.3. The impeller blade tip is located at the radius $r/R = 1$, for vertical position $2z/w$ ranging between -1 and 1. Moreover, the acquisitions are synchronized with the blade position and the measurement plane is acquired every 1° blade angle interval.

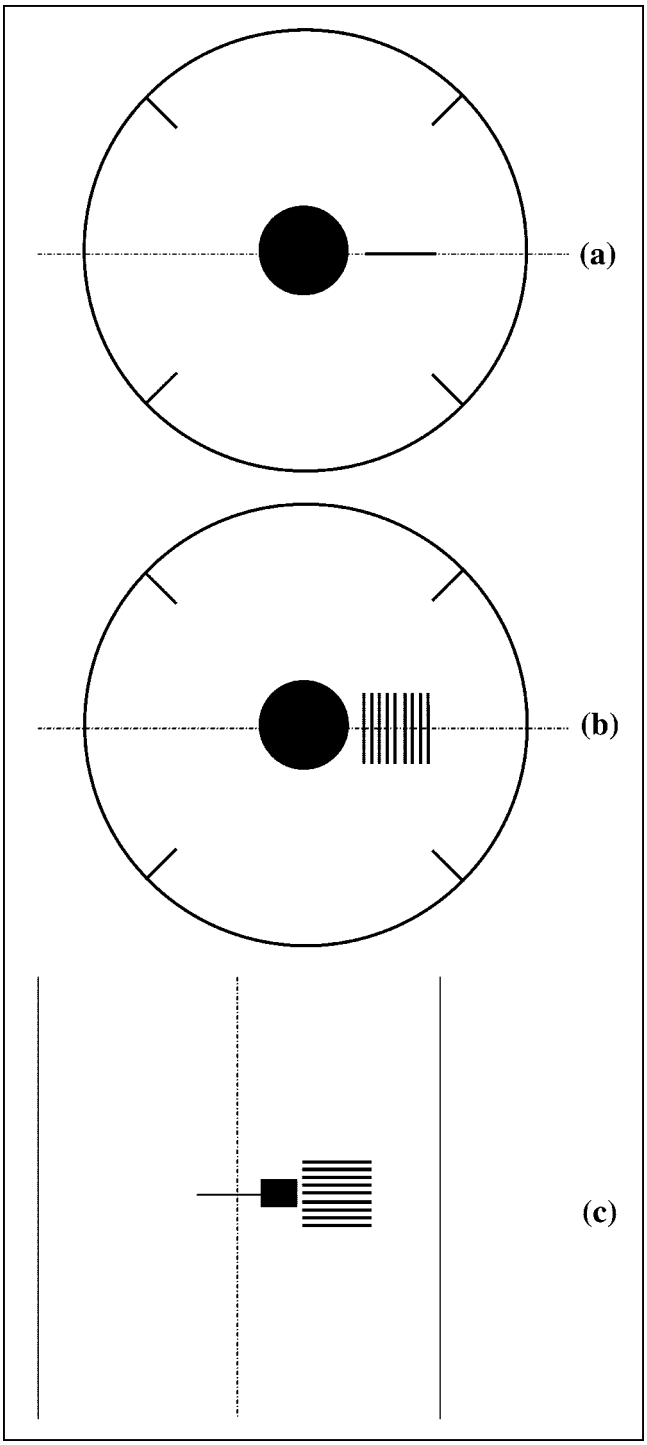

Figure 2. Measurement planes.

(a) vertical plane (X_1-X_3); (b) transversal planes (X_2-X_3); (c) horizontal planes (X_1-X_2).

Phase average treatment

A phase averaged treatment was performed to extract the mean flow, the organized fluctuating velocity and the turbulent velocity. A triple decomposition must be applied

$$U_i = \overline{U_i} + \tilde{u}_i + u_i' \tag{3}$$

where U_i is the instantaneous velocity, $\overline{U_i}$ is the averaged velocity, $\tilde{u}_i$ is the periodic fluctuation, and u_i' is the turbulent fluctuation.

The treatment is based on a series of two statistical averages. First, in a plane located at a fixed angle k relative to the blade position, the instantaneous information U_i^{lk} is decomposed into the averaged velocity of k plane $\langle U_i^k \rangle$ and the turbulent fluctuation $u_i'^k$ of k plane

$$U_i^{lk} = \langle U_i^k \rangle + u_i'^{lk}. \tag{4}$$

Statistics over 1,000 events (n_e) enable the following to be calculated in each k plane

- the average velocity of the k plane

$$\langle U_i^k \rangle = \sum_{l=1}^{n_e} \frac{U_i^{lk}}{n_e} \tag{5}$$

- the turbulent velocity correlation of k plane

$$\langle u_i'^k u_j'^k \rangle = \sum_{l=1}^{n_e} \frac{u_i'^{lk} u_j'^{lk}}{n_e} \tag{6}$$

Starting from the results in all the k planes ($n_p = 60$), a second statistical average enabled the mean velocity $\overline{U_i}$ of the flow and the periodic fluctuation $\tilde{u}_i^k$ to be calculated in each k plane

$$\langle U_i^k \rangle = \overline{U_i} + \tilde{u}_i^k \tag{7}$$

The periodic (or phase-averaged) motion has been verified to be divergence free (Escudié and Liné, 2003).

Vortex identification technique

The presence of a pressure minimum is the starting point for the method proposed by Jeong and Hussain (1995) for identifying a vortex region. According to the authors, the lack of correlation between the presence of a pressure minimum and the presence of a vortex core is due to two effects: *(i) unsteady straining, which can create a pressure minimum without involving a vortical or swirling motion, and (ii) viscous effects which can eliminate the pressure minimum in a flow with vortical motion.* By simply eliminating these effects from the calculations, the authors expect to obtain a better indicator for the existence of a vortex. The vortex region thus corresponds to local pressure minimum in a plane perpendicular to the vortex axis.

The following equation can be deduced from Jeong and Hussain's (1995) work (see Appendix A)

$$\Omega_{ik}\Omega_{kj} + S_{ik}S_{kj} = -\frac{1}{\rho}\frac{\partial^2 P}{\partial x_i \partial x_j} = -\frac{1}{\rho} p_{,ij} \tag{8}$$

with S, the deformation rate tensor

$$S_{ij} = \frac{1}{2}\left(\frac{\partial u_i}{\partial x_j} + \frac{\partial u_j}{\partial x_i}\right) \tag{9}$$

and Ω, the rotation rate tensor

$$\Omega_{ij} = \frac{1}{2}\left(\frac{\partial u_i}{\partial x_j} - \frac{\partial u_j}{\partial x_i}\right) \tag{10}$$

If two eigenvalues of the tensor $p_{,ij}$ are positive, this indicates the presence of a local pressure minimum. It corresponds to a vortex region. As a consequence, the tensor $S^2 + \Omega^2$ can be used to localize a vortex core: it requires two negative eigenvalues of tensor $S^2 + \Omega^2$. If λ_1, λ_2 and λ_3 are taken as the eigenvalues of $S^2 + \Omega^2$ and if $\lambda_1 \geq \lambda_2 \geq \lambda_3$, a vortex core corresponds to $\lambda_2 < 0$.

Results on Trailing Vortices Identification

Trailing vortex identification according to Jeong and Hussain technique

In the following, Jeong and Hussain's (1995) method will be considered as the reference technique for localizing the trailing vortex region in the measurement volume. The trailing vortex core is thus defined by the region where the second eigenvalue λ_2 of $S^2 + \Omega^2$ tensor is strictly negative. The $S^2 + \Omega^2$ tensor can be calculated from the experimental data bank in the volume limited as follows

$$1.07 \leq r/R \leq 1.6, \ -1.3 \leq 2z/w \leq 1.3, \ 0° \leq \text{angle} \leq 59$$

It is important to recall the basic steps of data acquisition and processing: the technique is based on the estimation of the eigenvalues of the deformation rate tensor and the rotation rate tensor. It means that the nine components of the velocity gradients have to be estimated. This estimation has to be made with phase averaging technique in order to determine the shape of the trailing vortices at each 1° behind a blade. Data correspond to one vertical-radial plane, nine vertical-tangential planes, and nine horizontal planes. Since phase average is performed each 1° between two blades of the impeller (60°), 60 sets of data are acquired: it represents 65,000 geometrical points distributed in the volume of liquid between two blades of the impeller. In addition, in each point, a statistic is performed in order to separate turbulence and mean flow (1,000 instantaneous velocity data in each point). All the above concerns data acquisition.

The treatment consists then in deriving the gradients of the velocity in the 65,000 nodes. Thus, the two tensors S and Ω are derived in each node. The eigenvalues of $S^2 + \Omega^2$ are determined at each node. The vortex is then localized. The maximum of second eigenvalue determines the center of the vortex in each one of the 60 vertical planes and, thus, the axis of the vortex (or its trajectory, in 3-D). Once the trajectory is derived, the unit vector along the trajectory is estimated. It is then possible to get correctly the vortex size in a plane normal to the trajectory of the vortex.

The measurement volume is, thus, made of $33 \times 33 \times 60$ nodes (65,000 experimental measurement points between two successive blades). In fact, this volume corresponds to the temporal evolution of the velocity data measured in a fixed vertical plane of measurement (33 rows $\times$ 33 columns). Data are synchronized with the position of one impeller blade relative to the plane of measurement. The impeller blade motion is periodic and the time interval between the passage of two successive blades is divided into 60 intervals. Thus, in a fixed plane of measurement, 60 events are analyzed between two successive blades. The measurement region is relatively far from the tank wall and hydrodynamics may be considered to be only marginally affected by the baffles. As a consequence, a spatial evolution of the velocity data in a moving frame of reference can be substituted to the temporal evolution of the velocity data measured in a fixed vertical plane. Thus, the 60 temporal events in a fixed plane can be considered as 60 spatial events in 60 planes located behind the blade.

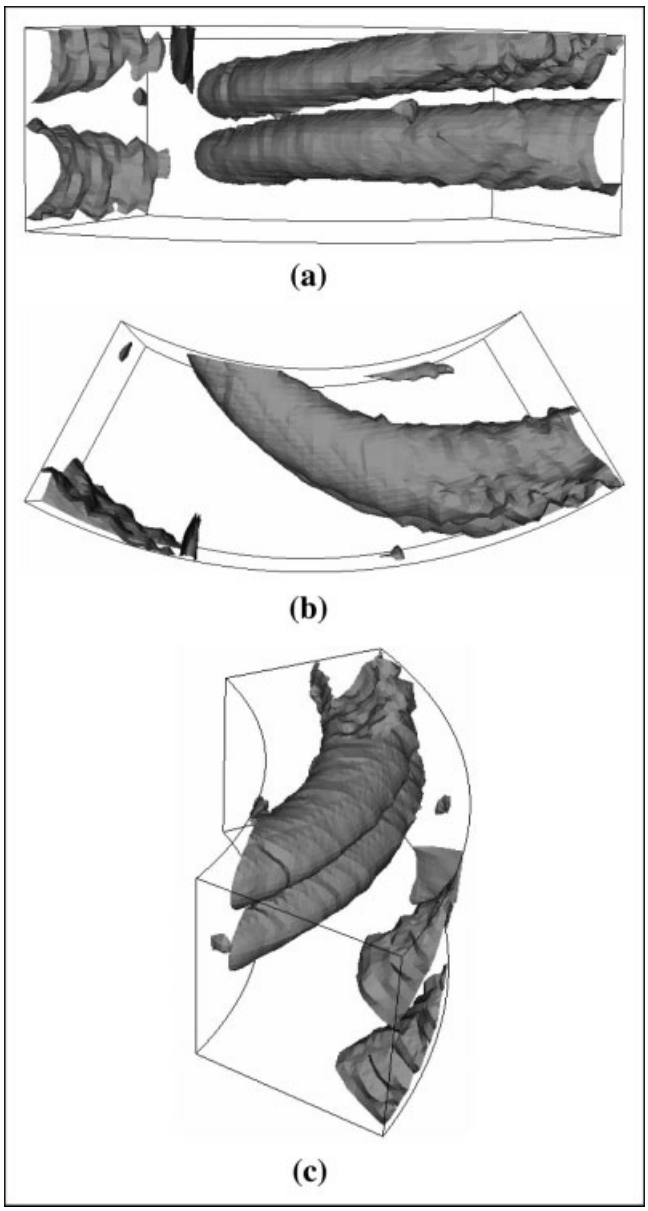

Figure 3. Visualization of the trailing vortices in the measurement volume with Jeong and Hussain's technique ($\lambda_2 < 0$).

(a) front view; (b) upper view; (c) perspective view.

Since the vortex region corresponds to $\lambda_2 < 0$, the vortex can be visualized by the surface $\lambda_2 = 0$, corresponding to the contour of the vortex region. Figures 3a, 3b, and 3c present the results in the measurement volume from the front view, the overhead view, and a perspective view, respectively. The impeller is rotating in the clockwise direction, as viewed from above. The averaged velocity in k plane $\langle U_i^k \rangle$ (Eq. 7 for the

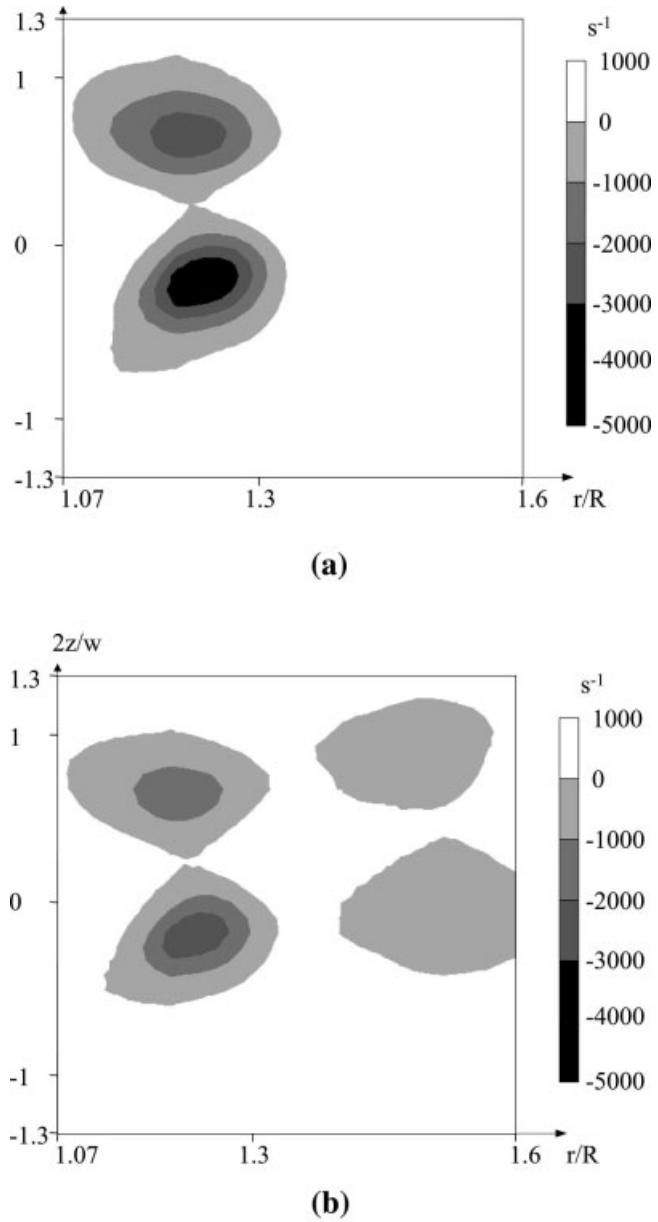

Figure 4. Location of the trailing vortices in vertical plane located at an angular position of 25° behind an impeller blade.

(a) λ_2 calculated from the phase-averaged velocity field $\langle U_i^k \rangle$; (b) λ_2 calculated from the velocity field of organized motion $\tilde{u}_i^k$.

definition) is used to calculate the velocity gradient tensor. Thus, the two trailing vortices can be easily located. Figure 3b shows that these vortices are generated from the backside of the impeller blade. A fluid volume separates the upper and the lower vortex region; the vortex pair is slightly displaced toward the top of the tank.

Figure 4 presents the distribution of the eigenvalue λ_2 in a vertical plane located at an angle of 25° behind a blade. It is important to point out that this plane is not perpendicular to the vortex axis; as a consequence, it is not easy to characterize the vortex in terms of size or spatial structure from this plane. The eigenvalue λ_2 can be calculated either from phase averaged velocity field $\langle U_i^k \rangle$ or the organized motion of the velocity field $\tilde{u}_i^k$. The resulting distributions are plotted in Figures 4a and 4b, respectively: the method for the identification of the main trailing vortices is the same. For a fixed angular position, λ_2 is larger in the lower vortex in both cases. The visualization of the eigenvalue λ_2 calculated from $\tilde{u}_i^k$ shows two additional vortex regions. These secondary vortices may be directly induced by the flow circulation in the main trailing vortices. However, the amplitude of λ_2 within these secondary coherent structures is small and does not exceed $-500\ s^{-2}$, whereas it is close to $-50{,}000\ s^{-2}$ in the main trailing vortex core.

Comparison of Reynolds and Hussain's technique with previous ones

In order to locate the trailing vortex core, two main approaches were followed in the past: the velocity flow pattern of the organized motion; a vorticity threshold.

Figures 5a–5d present the velocity field of organized motion ($\tilde{u}_i^k$) in a vertical plane situated at four angular positions of the blade compared to the measurement plane: the trailing vortices can only be visualized.

The vorticity magnitude was often used to localize the trailing vortices induced by a Rushton turbine (Derksen et al., 1999; Schaffer et al., 2000). This parameter is a characteristic of the fluid motion inside the vortex. Since measurements are performed in a vertical plane, only one component of the vorticity vector is usually estimated, normal to this plane. In a vertical plane (angle k), the vorticity magnitude (ω) was calculated using the following relationship

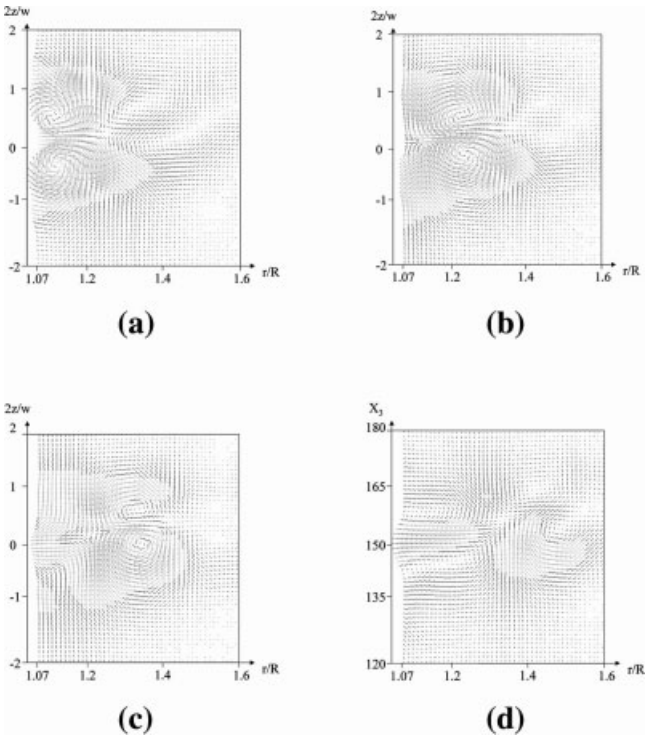

Figure 5. Velocity field of organized motion in a vertical plane for four angular positions.

(a) 15°; (b) 25°; (c) 35°; (d) 50°.

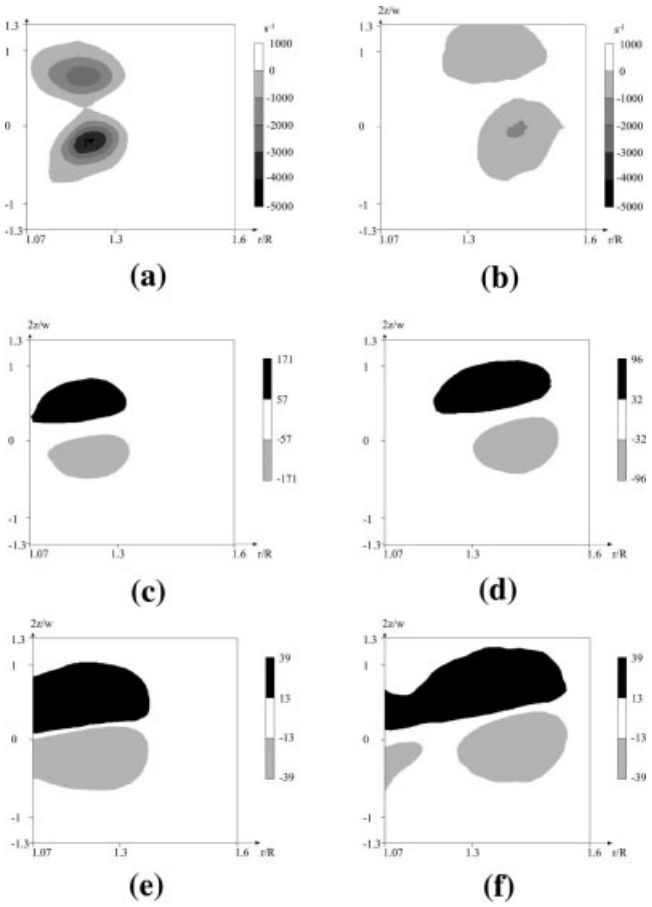

Figure 6. Trailing vortex identification with vorticity magnitude in a vertical plane located at two angular positions behind an impeller blade.

(a) reference: Jeong and Hussain's technique ($\lambda_2 < 0$) (angular position = 25°); (b) reference: Jeong and Hussain's technique ($\lambda_2 < 0$) (angular position = 40°); (c) dimensionless threshold value $\xi_c = 60$ (angular position = 25°); (d) dimensionless threshold value $\xi_c = 60$ (angular position = 40°); (e) dimensionless threshold value $\xi_c = 13$ (Schaffer et al., 2000) (angular position = 25°); (f) dimensionless threshold value $\xi_c = 13$ (Schaffer et al., 2000) (angular position = 40°).

$$\omega = \frac{\partial \langle U_1^k \rangle}{\partial x_3} - \frac{\partial \langle U_3^k \rangle}{\partial x_1} \tag{11}$$

In order to define a vortex region, it is necessary to fix a threshold on the vorticity magnitude, as proposed by Schaffer et al. (2000).

Following the method of Jeong and Hussain, the vortex region was first identified by finding the regions of negative value of λ_2. Results are plotted in a given vertical plane, 25° behind a blade. The corresponding trailing vortex region is plotted in Figure 6a. Different values of vorticity magnitude threshold have been tested in order to determine a vortex region close to the region identified on Figure 6a: Figure 6c corresponds to the vorticity field, with a dimensionless threshold value of $\xi_c = \omega_c T/U_{tip} = 57$. It is interesting to compare this threshold to the value recommended by Schaffer et al. (2000): they proposed a threshold $\xi_c = 13$. The corresponding region has been plotted in Figure 6e: it does not correspond to the trailing vortex. This threshold value does overestimate the size of the vortex.

A second set of figures has been plotted for another vertical plane, 40° behind the blade. Figure 6b corresponds to the vortex region identified according to the Jeong and Hussain method. Figure 6d corresponds to a vorticity magnitude threshold, which enables the determination of a vortex region corresponding to the region identified in Figure 6b. In this plane, the dimensionless threshold value is equal to $\xi_c = 35$. It is smaller than the threshold value fitting the vortex region in the previous plane: the threshold value seems not to be constant. It is larger than the value proposed by Schaffer et al. (2000) given by $\xi_c = 13$; the region corresponding to this last value has been plotted in Figure 6f: it overestimates again the size of the vortex. The shape of the region is wrong.

The method based on vorticity magnitude is easy to develop: only two components of the velocity in one plane are necessary. The previous results demonstrate the inability of this method (based on a constant vorticity threshold) to identify trailing vortex regions. The technique of Jeong and Hussain is more difficult to develop since it requires a large volume of data to be acquired and to be treated. It seems that the technique of Jeong and Hussain is the only one able to identify trailing vortices.

Characteristics of Trailing Vortices in Mixing Tanks

The displacement of the vortex center describes a trajectory, which is called here the vortex axis. In order to visualize the vortex axis, the location of the minimum value of λ_2 in the trailing vortex region will be considered as the reference one. In the past, different techniques were developed to determine the vortex trajectory. In a vertical plane of measurement, the vortex center was located by the position where the velocity of the organized motion is equal to 0 ("null velocity technique"). In other words, the trailing vortex center was defined by the location of the maximum vorticity magnitude.

The three identification schemes of vortex center localization have been tested in this article: Jeong and Hussain's technique (considered as the reference), null velocity location, and maximum vorticity. The maximum of the absolute value of the second eigenvalue λ_2 determines the center of the vortex in each one of the 60 vertical planes. It, thus, locates thus the axis of the vortex. Figures 7a and 7b present the vertical displacement of the trailing vortices vs. the angular position relative to the blade. The radial displacement is plotted in Figures 7c and 7d. The null velocity location method is compared to the Jeong and Hussain technique in Figures 7a and 7c. The maximum vorticity method is compared to the Jeong and Hussain technique in Figures 7b and 7d. The null velocity location method does not enable the trajectory of the vortices to be drawn correctly in the measurement volume. When the vortices are far from the impeller ($r/R = 1.6$), the difference in the trajectory between this technique and the reference one is about 5 mm ($w/6$). As far as the vortex axis is concerned, the difference between the vorticity magnitude method and reference one is small.

Considering the overall trend of the trailing vortex trajectory, they have a slight vertical motion directed toward the tank top. The distance between the upper and the lower vortex is

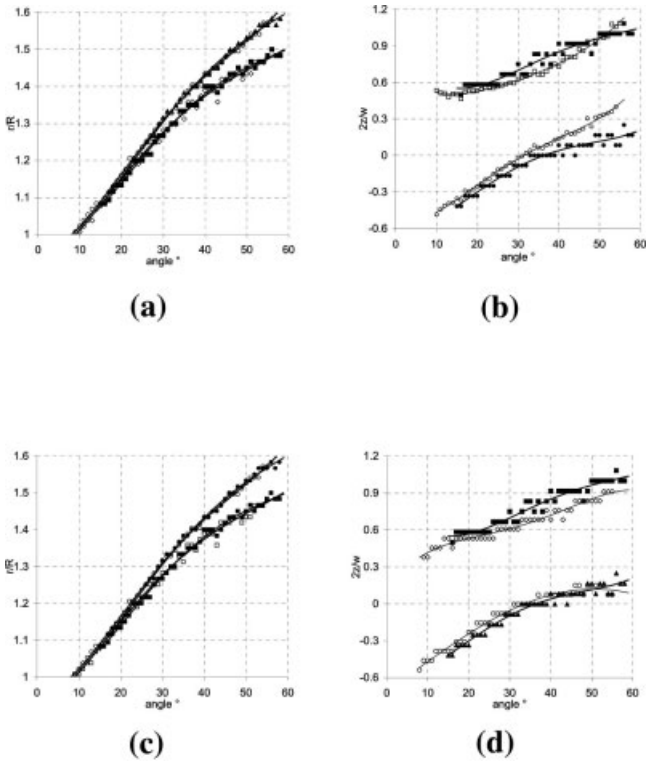

Figure 7. Displacement of the trailing vortices derived from three techniques.

Filled symbol: λ_2 technique (upper vortex, ▲ lower vortex) (Figure a, b, c and d); open symbol: null velocity technique (□ upper vortex, △ lower vortex) (Figure a and c) vorticity technique (◇ upper vortex, ○ lower vortex) (Figure b and d). (a) Vertical displacement: λ_2 technique and «null velocity technique»; (b) Vertical displacement: λ_2 technique and vorticity technique; (c) Radial displacement: λ_2 technique and «null velocity technique»; (d) Radial displacement: λ_2 technique and vorticity technique.

constant and equals 12.5 mm (0.4 w). In terms of the radial displacement in the jet (Figure 7b), the lower vortex is shifted slightly outwards compared to the upper one. For an angular position of 55°, the distance is about 0.2 w.

In Figure 8, the upper and lower vortex axes are compared to previous works (Van't Riet and Smith, 1975; Yianneskis et al., 1987; Stoots and Calabrese, 1995; Lee and Yianneskis, 1998; Derksen et al., 1999). These works correspond to different data sets. The vortex displacement in the present work lies between the data of Van't Riet and Smith (1975) and Stoots and Calabrese (1995). The differences can be attributed to the characteristics of the stirred tank (clearance C, blade or disk thickness) rather than to the technique of vortex axis localization. The geometrical parameters of the tank strongly affect the mean flow generated in the stream of the Rushton turbine (Rutherford et al., 1996; Escudié and Liné, 2003) and the trajectory of the vortices can be assumed to be linked to the mean velocity near the impeller blade. Indeed, the measurements plotted in Figure 8 agree in terms of the location of the trailing vortices near the impeller blade ($r/R = 1$) where they are generated. As the mean velocity gradient has a high value in the impeller jet, a small difference in the mean velocity in the blade tip region can explain the trajectory difference for larger radial positions. The link between the trajectory of the vortices and the velocity field induced by the impeller will be established in the next paragraph.

Trailing vortex trajectory and mean flow

The objective of this section is to establish the relation between the trailing vortex axis in the tank and the flow generated by the Rushton turbine. It can be shown that the vortices move according to the phase-averaged flow field ($\langle U_i^k \rangle = \overline{U_i} + \tilde{u}_i^k$). Thanks to Jeong and Hussain's technique, the displacements of the lower and upper trailing vortices were determined precisely in the volume of the tank in terms of the maximum negative value of λ_2. The resulting vortex axis can be shown to follow the trajectory of fluid particles determined from the phase-averaged velocity field within the tank.

The «Ensight» software is used to visualize the trailing vortex axis determined from Jeong and Hussain's technique. In addition, starting from the location of the two vortices at the impeller tip ($r/R = 1$) (starting point), it is possible to visualize the trajectory of the fluid particle using the 3-D field ($\langle U_i^k \rangle$). Figures 9a, 9b, and 9c present the measurement volume from the front view, the overhead view, and a perspective view, respectively. A similarity between the location of the vortex axis and the trajectory of fluid particles can be observed, particularly for the lower trailing vortex. Concerning the upper vortex, the fluid particle trajectory coincides with the vortex core in the region close to the impeller tip; when the radial position increases, a small difference occurs for the vertical location whereas the radial displacement is correctly estimated. The difference can be attributed to a discrepancy in the starting point location of the trajectory. It is possible to conclude that the trailing vortices move according to the phase-averaged velocity field ($\langle U_i^k \rangle$). Thus, the trailing vortex axis follows a fluid particle trajectory of the phase-averaged velocity field.

Once the identification of the trailing vortex has been performed, the objective is now to characterize these vortices: their size and the velocity circulation within the trailing vortex (Γ). Once the trajectory is derived, the unit vector along the trajectory is estimated. It is then possible to determine correctly the vortex size in a plane normal to the trajectory of the vortex and the velocity circulation.

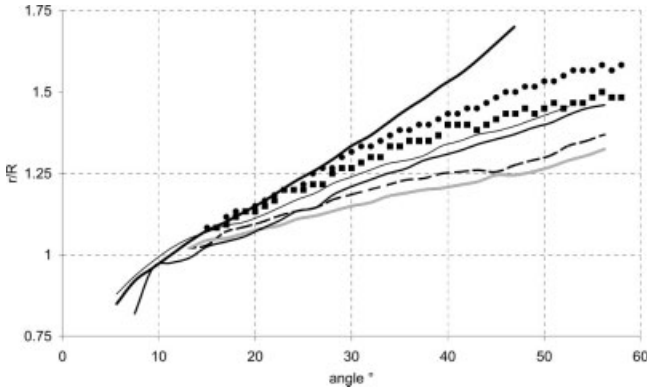

Figure 8. Comparison of the loci of the axis of trailing vortex.

■ upper vortex, ● lower vortex, —— Van't Riet and Smith (1975); — — Yianneskis et al. (1987) —— Stoots and Calabrese (1995); —— Lee and Yiannekis (1998); —— Derksen et al. (1999).

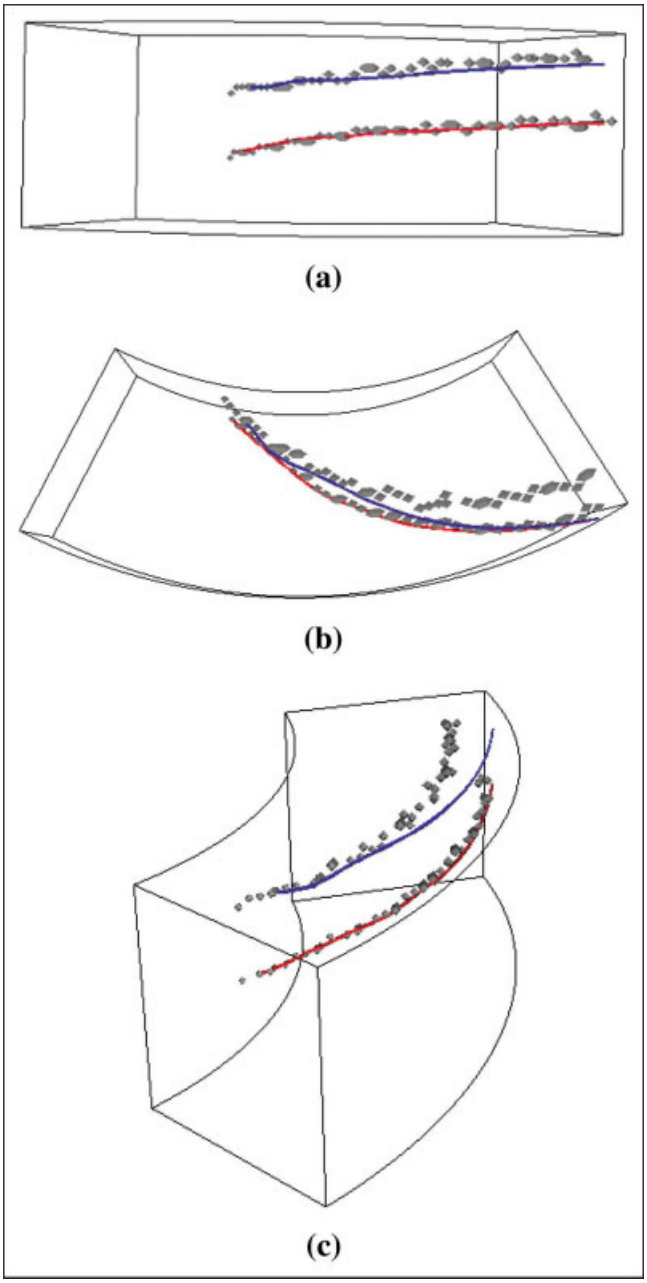

Figure 9. Relation between trailing vortex axis and 3-D flow field.

◆ Trailing vortex detection from Jeong and Hussain's technique; —— Trajectory of a fluid particle using 3-D phase-averaged field.

Trailing vortex size

The trailing vortex size can be determined from its projected surface (S_p) in the plane perpendicular to the vortex axis (plane P). The equation of fluid particle trajectory can be calculated with Ensight Software. The trajectory of the fluid particle coincides with the vortex axis, so the equation of the trajectory also describes the vortex axis. Consequently, in each point situated on this trajectory, the plane P perpendicular to the vortex axis and its normal vector $\vec{n}$ can be defined. In each plane P, the vortex surface S_p can be identified as the region where the second eigenvalue λ_2 of $S^2 + \Omega^2$ tensor is negative.

Figure 10a presents the vortex surface S_p vs. the curvilinear abscissa δ. δ corresponds to the distance covered by the vortex center between its origin behind the blade ($r/R = 1$) and the measurement point situated on the vortex axis. When the trailing vortex moves away from the impeller, its surface area S_p remains constant, at 230 mm^2. Assuming the trailing vortex section to be circular, the vortex diameter is 17 mm, which is close to $w/2$ (w, blade height). Once the size of the vortex has been determined, the velocity circulation can be derived.

Velocity circulation within the trailing vortex

The velocity circulation within a vortex (Γ) can be defined as follows

$$\Gamma = \int_{S_p} \vec{\nabla} \times \vec{\tilde{u}} \cdot \vec{n} ds \tag{12}$$

with $\vec{n}$ the normal vector of the plane P, S_p the vortex surface projected onto plane P and $\vec{\tilde{u}}$ the velocity vector of the organized motion.

Γ represents the flux of the rotational vector of the organized velocity ($\vec{\Omega} = \nabla \times \vec{\tilde{u}}$) through a vortex surface (S_p). In the case of an inviscid fluid, the circulation Γ remains constant

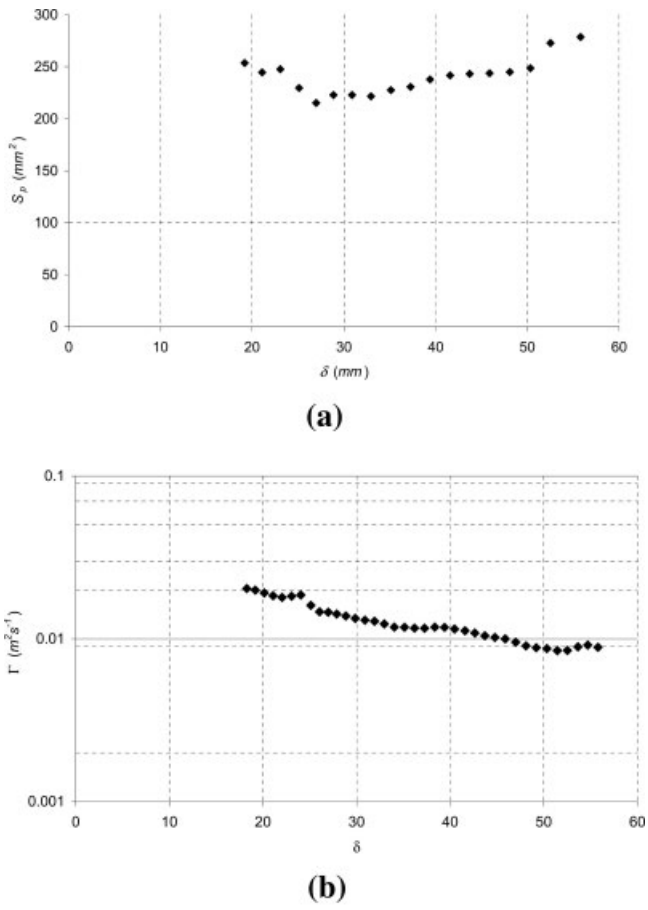

Figure 10. Trailing vortex characteristics.

(a) the vortex surface S_p; (b) the velocity circulation within the trailing vortex Γ.

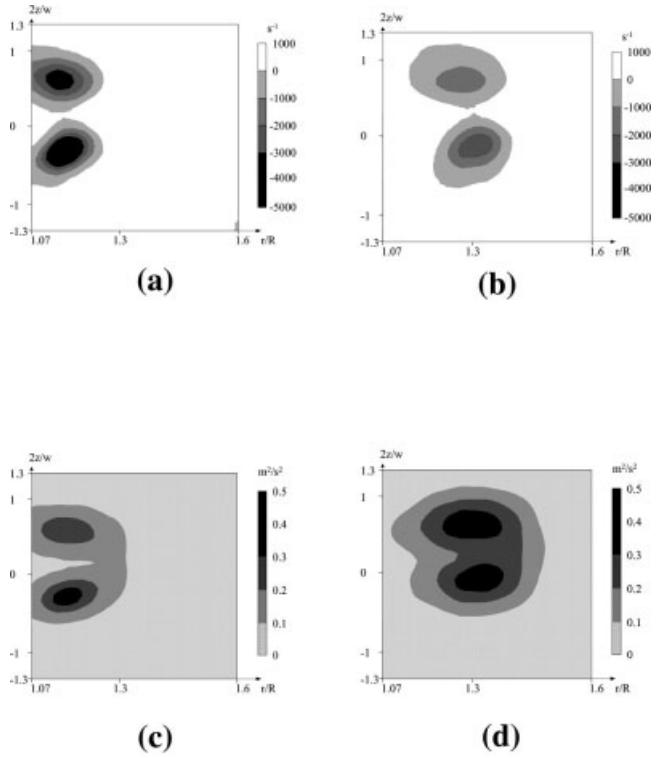

Figure 11. Interaction between trailing vortex location and turbulence.

(a) λ_2 for the angular position 20°; (b) λ_2 for the angular position 30°; (c) k for the angular position 20°; (d) k for the angular position 30°.

with the vortex displacement. In the case of the upper trailing vortex, the normal vector $\vec{n}$ of plane P can be defined starting from the equation of the vortex trajectory. In addition, in this plane, the vortex core area and the vorticity vector $\vec{\Omega}$ can be derived, and, thus, the velocity circulation (Γ) can be calculated. Figure 10b presents Γ vs. the curvilinear abscise δ. When the vortex moves away from the impeller, the velocity circulation within a vortex (Γ) drops sharply. The velocity circulation within the vortex is not conservative. This can be understood since the organized motion transfers kinetic energy to turbulence. Escudié and Liné (2003) quantified the term for the exchange of kinetic energy between organized and turbulent motion and concluded that this term has the same order of magnitude as the term of exchange of kinetic energy between mean and turbulent motion (classical production term). This interaction can now be illustrated. The decomposition technique enables the following to be visualized: the level of the turbulent kinetic energy (k); the trailing vortex region ($\lambda_2 < 0$).

In Figure 11, these two characteristics are plotted for two angular positions (20° and 30°) in a vertical plane. The turbulent kinetic energy is localized in the region of the trailing vortex core because the transfer of kinetic energy between organized and turbulent flows ($\overline{Tot}$) is located in this region (Escudié and Liné, 2003). Starting from the kinetic energy balance of the turbulent motion (Reynolds and Hussain, 1972), the kinetic energy transfer $\overline{Tot}$ between organized motion and turbulence is identified as

$$\overline{Tot} = \overline{\left(-\langle u_i' u_j' \rangle \frac{\partial \tilde{u}_i}{\partial x_j} \right)} \tag{13}$$

with $\langle u_i' u_j' \rangle$ the phase-average turbulent Reynolds stress and $\partial \tilde{u}_i / \partial x_j$ the gradient of the organized velocity (trailing vortices). The magnitude of the gradient $\partial \tilde{u}_i / \partial x_j$ is large in a vortex zone. In addition, the Reynolds stresses $\langle u_i' u_j' \rangle$ are spatially correlated to the trailing vortices core (Lee and Yianneskis, 1998; Sharp and Adrian, 2001; Escudié, 2001; Bouyer, 2002). As a consequence, the transfer $\overline{Tot}$ between organized motion and turbulence is located in the region identified as a trailing vortex region by the Jeong and Hussain technique.

Summary and Conclusion

The PIV technique was used to study a standard cylindrical tank equipped with a Rushton turbine.

The objectives of this article were to identify and characterize the trailing vortices generated behind the impeller blade. This study is based on an objective definition of a vortical structure proposed by Jeong and Hussain (1995). This definition is based on the eigenvalues of the tensor $S^2 + \Omega^2$, where S and Ω are, respectively, the symmetric and the antisymmetric parts of the velocity gradient tensor $\nabla \otimes u$. If the second eigenvalue λ_2 of the tensor $S^2 + \Omega^2$ is negative, then the measurement point is located in a vortex region.

In the first part of this study, this technique was used to localize the trailing vortex in the measurement volume situated between two successive impeller blades. A fluid volume that separates the upper and the lower vortex was observed, and the vortex pair was slightly directed toward the top of the tank. This technique was compared to a previous one: the vorticity magnitude, which is often used to localize the trailing vortex. This method is based on a dimensionless threshold value (ξ_c) to be fixed arbitrarily and to identify objectively a vortical region. The results demonstrated clearly the inability of this method to identify objectively, because the result depended on the threshold value (ξ_c).

In addition, the axis of the trailing vortices was drawn in the measurement volume. Starting from the velocity field of the organized motion in a vertical measurement plane, the vortex center was localized in terms of null vertical velocity. However, the trajectory of the vortex derived from this technique was inaccurate. The technique of Jeong and Hussain enables the axis of the vortex to be determined in terms of the location of the maximum absolute value of the second negative eigenvalue. The trajectory could also have been obtained with the maximum vorticity method. The relation between the trailing vortex axis and the flow generated by the turbine was then emphasized. The displacement of the upper and lower axis follows the trajectory of a fluid particle calculated from the phase-averaged velocity field $\langle U_i^k \rangle$.

The second objective was to characterize the trailing vortices in the impeller stream. Once the trajectory was derived, the unit vector along the trajectory was estimated. It was then possible to correctly obtain the vortex size in a plane normal to the trajectory of the vortex. The size of the projected surface S_p of the lower vortex in the plane perpendicular to the vortex axis appeared to be constant: the size corresponds to a diameter closed to $w/2$ if the vortex is assumed to be cylindrical. The

velocity circulation within the upper trailing vortex (Γ) was calculated, and it was shown to decrease when it moved away from the impeller. The fact that the velocity circulation (Γ) does not remain constant can be understood, because the organized motion transfers a certain amount of kinetic energy to the turbulent motion. The region characterized by a strong turbulent kinetic energy transfer was confirmed to be situated in the region identified as the trailing vortex core by the Jeong and Hussain technique.

Acknowledgment

The financial support provided by Ministère de l'Education Nationale et de la Recherche and Région Midi-Pyrénées is gratefully acknowledged.

Notation

B = baffle width, m
C = impeller clearance, m
d_p = seeding particle diameter, m
D = impeller diameter, m
H = liquid height in the tank, m
k = turbulent kinetic energy, m^2/s^2
$\tilde{k}$ = organized kinetic energy, m^2/s^2
n_e = acquisition number per measurement plane
n_p = plane number between two successive blades
N = rotational speed, rev/s
Re = Reynolds number
r/R = dimensionless radial position
S = symmetrical part of the velocity gradient tensor, 1/s
S_p = projected surface in the plane perpendicular to the vortex trajectory, m^2
t_b = blade thickness, m
t_d = disk thickness, m
T = tank diameter, m
U, u = velocity component, m/s
U_{tip} = tip velocity, m/s
$\langle U_i^k(M, t)\rangle$ = phase averaged velocity in the k plane, m/s
$\tilde{u}_i^k(M, t)$ = organized periodic velocity in the k plane, m/s
w = impeller width, m
z/w = dimensionless vertical position
λ_T = Taylor microscale, m
ν = kinematic viscosity, m^2/s
ρ = fluid density, kg/m^3
λ_i = eigenvalues of the tensor $S^2 + \Omega^2$, $1/s^2$
Ω = antisymmetric parts of the velocity gradient tensor, 1/s
∇u = velocity gradient tensor, 1/s
ω = dimensional vorticity in the vertical plane, 1/s
ξ = dimensionless vorticity in the vertical plane
z/w = dimensionless vertical position
Γ = the velocity circulation within the Trailing vortex, m^2/s^2
δ = distance covered by the vortex core, m

Literature Cited

Bouyer, D., "Analyse Expérimentale de la Floculation: Influence de l'Hydrodynamique sur les Phénomènes d'agglomération et de Rupture," Thèse de Doctorat de l'Institut National des Sciences Appliquées, Toulouse (2002).

Costes, J., and J. P. Couderc, "Influence of the Size of the Units: I Mean Flow and Turbulence," *Chem. Eng. Sci.,* **43**(10), 2751 (1988).

Cutter, L. A., "Flow and Turbulence in a Stirred Tank," *AIChE J.,* **12,** 35 (1966).

Derksen, J. J., M. S. Doelman, and H. E. A. Van Den Akker, "Three-dimensional LDA Measurements in the Impeller Region of a Turbulently Stirred Tank," *Exp. in Fluids,* **27,** 522 (1999).

Escudié, R., "Structure Locale de l'Hydrodynamique Générée par une Turbine de Rushton," Thèse de Doctorat de l'Institut National des Sciences Appliquées, Toulouse (2001).

Escudié, R., and A. Liné, "Experimental Analysis of Hydrodynamics in a Radially Agitated Tank," *AIChE J.,* **49**(3), 585 (2003).

Jeong, J., and F. Hussain, "On the Identification of a Vortex," *J. Fluid Mech.,* **285,** 69 (1995).

Keane, R. D., and R. J. Adrian, "Theory of Cross-Correlation Analysis of P.I.V. Images," *Appl. Scientific Res.,* **49,** 191 (1992).

Lee, K. C., and M. Yiannekis, "Turbulence Properties of the Impeller Stream of a Rushton Turbine," *AIChE J.,* **44**(1), 13 (1998).

Mahouast, M., G. Cognet, and R. David, "Two-Component LDV Measurements in a Stirred Tank," *AIChE J.,* **35**(11), 1770 (1989).

Mujumbar, A. S., B. Huang, D. Wolf, M. E. Weber, and W. S. M. Douglas, "Turbulence Parameters in a Stirred Tank," *Can. J. Chem. Eng.,* **48,** 475 (1970).

Ranade, V. R., M. Perrard, N. Le Sauze, C. Xuereb, and J. Bertrand, "Trailing Vortices of Rushton Turbine: PIV Measurements and CFD Simulations with Snapshot Approach," *TransIChemE,* **79** (Part A), 3 (2001).

Reynolds, W. C., and A. K. M. F. Hussain, "The Mechanics of an Organized Wave in Turbulent Shear Flow. Part 3. Theoretical Models and Comparisons with Experiments," *J. Fluid Mech.,* **54** (Part 2), 263 (1972).

Rutherford, K., M. S. Mahmoudi, K. C. Lee, and M. Yianneskis, "The Influence of Rushton Impeller Blade and Disk Thickness on the Mixing Characteristics of the Stirred Vessels," *TransIChemE,* **74** (Part A), 369 (1996).

Schaffer, M., J. Yu, B. Geneger, and F. Durst, "Turbulence Generation by Different Types of Impellers," *Proc. of the 10th European Conf.,* Delft, The Netherlands, H. E. A. van den Akker and J. J. Derksen, eds., Elsevier, 9 (July 2–5, 2000).

Schaffer, M., M. Hofken, and F. Durst, "Detailed LDV Measurements for the Visualisation of the Flow Field within a Stirred-Tank Reactor Equipped with a Rushton Turbine," *TransIChemE,* **75** (Part A), 729 (1997).

Sharp, K. V., and R. J. Adrian, "PIV Study of Small-Scale Flow Structure around a Rushton Turbine," *AIChE J.,* **47**(4), 766 (2001).

Stoots, C., and R. V. Calabrese, "Mean Velocity Field Relative to a Rushton Turbine Blade," *AIChE J.,* **41**(1), 1 (1995).

Van der Molen, K., and H. R. E. Van Maanen, "Laser-Doppler Measurements of the Turbulent Flow in Stirred Vessels to Establish Scaling Rules," *Chem. Eng. Sci.,* **33,** 1161 (1978).

Van't Riet, K., and J. M. Smith, "The Behaviour of Gas-Liquid Mixtures near Rushton Turbine Blades," *Chem. Eng. Sci.,* **28,** 1031 (1973).

Van't Riet, K., and J. M. Smith, "The Trailing Vortex System Produced by Rushton Turbine Agitators," *Chem. Eng. Sci.,* **30,** 1093 (1975).

Van't Riet, K., W. Bruijn, and J. M. Smith, "Real and Pseudo-Turbulence in the Discharge Stream from a Rushton Turbine," *Chem. Eng. Sci.,* **31,** 407 (1976).

Wu, H., and G. K. Patterson, "Laser-Doppler Measurements of Turbulent Flow Parameters in a Stirred Mixer," *Chem. Eng. Sci.,* **44,** 2207 (1989).

Yianneskis, M., and J. H. Whitelaw, "On the Structure of the Trailing Vortices around the Rushton Turbine Blades," *TransIChemE,* **71** (Part A), 543 (1993).

Yianneskis, M., "Trailing Vortex, Mean Flow and Turbulence Modification through Impeller Blade Design in a Stirred Reactors," *10th European Conf. on Mixing,* Delft, 1 (2000).

Yianneskis, M., Z. Popiolek, and J. H. Whitelaw, "An Experimental Study of the Steady and Unsteady Flow Characteristics of Stirred Reactors," *J. Fluid Mech.,* **175,** 537 (1987).

Appendix

The definition is based on the Navier-Stokes equation

$$\frac{Du_i}{D_t} = -\frac{1}{\rho}\frac{\partial P}{\partial x_i} + \nu_k \frac{\partial u_i}{\partial x_k} + g_i \tag{A1}$$

The gradient of the Navier-Stokes equation is taken

$$\frac{\partial}{\partial x_j}\left(\frac{Du_i}{Dt}\right) = \frac{D}{Dt}\left(\frac{\partial u_i}{\partial x_j}\right) + {}_k \frac{\partial u_k}{\partial x_j}\frac{\partial u_i}{\partial x_k} \tag{A2}$$

The velocity gradient tensor ∇u can be divided into symmetrical S and antisymmetrical Ω parts, as follows

$$\frac{\partial u_i}{\partial x_j} = S_{ij} + \Omega_{ij} \tag{A3}$$

with S, the deformation rate tensor

$$S_{ij} = \frac{1}{2}\left(\frac{\partial u_i}{\partial x_j} + \frac{\partial u_j}{\partial x_i}\right) \tag{A4}$$

and Ω, the rotation rate tensor

$$\Omega_{ij} = \frac{1}{2}\left(\frac{\partial u_i}{\partial x_j} - \frac{\partial u_j}{\partial x_i}\right) \tag{A5}$$

Substituting S_{ij} and Ω_{ij} components, Eq. 16 becomes

$$\frac{\partial}{\partial x_j}\left(\frac{Du_i}{Dt}\right) = \frac{D}{Dt}(S_{ij} + \Omega_{ij}) + {}_k(S_{kj} + \Omega_{ik})(S_{ik} + \Omega_{ik}) \tag{A6}$$

It is possible to distinguish the symmetric and antisymmetric parts of this equation

$$\frac{\partial}{\partial x_j}\left(\frac{Du_i}{Dt}\right) = \left[\frac{D}{Dt}(S_{ij}) + \Omega_{ik}\Omega_{kj} + S_{ik}S_{kj}\right] + \left[\frac{D}{Dt}(\Omega_{ij}) + \Omega_{ik}S_{kj} + S_{ik}\Omega_{kj}\right] \tag{A7}$$

Starting from Eq. 7, the symmetric part of Eq. 12 is

$$\frac{D}{Dt}(S_{ij}) + \Omega_{ik}\Omega_{kj} + S_{ik}S_{kj} = -\frac{1}{\rho}\frac{\partial^2 P}{\partial x_i \partial x_j} + \nu_k \frac{\partial^2 S_{ij}}{\partial x_k^2} \tag{A8}$$

The first term represents the unsteady irrotational straining and the last term represents the viscous effects. If the flow is steady and disregarding the viscous terms, it can be deduced that

$$\Omega_{ik}\Omega_{kj} + S_{ik}S_{kj} = -\frac{1}{\rho}\frac{\partial^2 P}{\partial x_i \partial x_j} = -\frac{1}{\rho}p_{,ij} \tag{A9}$$

Manuscript received Oct. 18, 2002, and revision received Oct. 11, 2003.